arXiv:1806.09182v1 [hep-ex] 24 Jun 2018

Evidence of charged $\Xi_c(2930)$ and updated measurement of $B^0 \to K^0 \Lambda_c^+ \bar{\Lambda}_c^-$ at Belle

Y. B. Li,[68] C. P. Shen,[2] I. Adachi,[19,15] H. Aihara,[81] S. Al Said,[77,38] D. M. Asner,[4] T. Aushev,[54] R. Ayad,[77] V. Babu,[78] I. Badhrees,[77,37] S. Bahinipati,[24] Y. Ban,[68] V. Bansal,[66] P. Behera,[27] C. Beleño,[14] V. Bhardwaj,[23] B. Bhuyan,[25] J. Biswal,[34] A. Bobrov,[5,64] A. Bozek,[61] M. Bračko,[49,34] T. E. Browder,[18] L. Cao,[36] D. Červenkov,[6] P. Chang,[60] V. Chekelian,[50] A. Chen,[58] B. G. Cheon,[17] K. Chilikin,[44] K. Cho,[39] S.-K. Choi,[16] Y. Choi,[75] S. Choudhury,[26] D. Cinabro,[85] S. Cunliffe,[9] N. Dash,[24] S. Di Carlo,[42] J. Dingfelder,[3] Z. Doležal,[6] T. V. Dong,[19,15] Z. Drásal,[6] S. Eidelman,[5,64,44] D. Epifanov,[5,64] J. E. Fast,[66] B. G. Fulsom,[66] R. Garg,[67] V. Gaur,[84] N. Gabyshev,[5,64] A. Garmash,[5,64] M. Gelb,[36] A. Giri,[26] P. Goldenzweig,[36] B. Golob,[45,34] J. Haba,[19,15] K. Hayasaka,[63] S. Hirose,[55] W.-S. Hou,[60] T. Iijima,[56,55] K. Inami,[55] G. Inguglia,[9] A. Ishikawa,[80] R. Itoh,[19,15] M. Iwasaki,[65] Y. Iwasaki,[19] W. W. Jacobs,[28] I. Jaegle,[10] H. B. Jeon,[41] S. Jia,[2] Y. Jin,[81] K. K. Joo,[7] A. B. Kaliyar,[27] K. H. Kang,[41] Y. Kato,[55] T. Kawasaki,[63] D. Y. Kim,[73] J. B. Kim,[40] S. H. Kim,[17] K. Kinoshita,[8] P. Kodyš,[6] S. Korpar,[49,34] D. Kotchetkov,[18] P. Križan,[45,34] R. Kroeger,[52] P. Krokovny,[5,64] T. Kuhr,[46] Y.-J. Kwon,[87] J. S. Lange,[12] I. S. Lee,[17] S. C. Lee,[41] L. K. Li,[29] L. Li Gioi,[50] J. Libby,[27] D. Liventsev,[84,19] T. Luo,[11] D. Matvienko,[5,64,44] M. Merola,[31,57] H. Miyata,[63] R. Mizuk,[44,53,54] H. K. Moon,[40] T. Mori,[55] R. Mussa,[32] E. Nakano,[65] T. Nanut,[34] K. J. Nath,[25] Z. Natkaniec,[61] M. Nayak,[85,19] N. K. Nisar,[69] S. Nishida,[19,15] K. Nishimura,[18] K. Ogawa,[63] S. Okuno,[35] H. Ono,[62,63] P. Pakhlov,[44,53] G. Pakhlova,[44,54] B. Pal,[4] S. Pardi,[31] H. Park,[41] S. Paul,[79] T. K. Pedlar,[47] R. Pestotnik,[34] L. E. Piilonen,[84] V. Popov,[44,54] E. Prencipe,[21] A. Rostomyan,[9] G. Russo,[31] Y. Sakai,[19,15] M. Salehi,[48,46] S. Sandilya,[8] L. Santelj,[19] T. Sanuki,[80] V. Savinov,[69] O. Schneider,[43] G. Schnell,[1,22] C. Schwanda,[30] Y. Seino,[63] K. Senyo,[86] O. Seon,[55] M. E. Sevior,[51] T.-A. Shibata,[82] J.-G. Shiu,[60] E. Solovieva,[44,54] M. Starič,[34] J. F. Strube,[66] M. Sumihama,[13] T. Sumiyoshi,[83] M. Takizawa,[72,20,70] U. Tamponi,[32] K. Tanida,[33] F. Tenchini,[51] M. Uchida,[82] T. Uglov,[44,54] Y. Unno,[17] S. Uno,[19,15] Y. Usov,[5,64] C. Van Hulse,[1] R. Van Tonder,[36] G. Varner,[18] K. E. Varvell,[76] V. Vorobyev,[5,64,44] E. Waheed,[51] B. Wang,[8] C. H. Wang,[59] M.-Z. Wang,[60] P. Wang,[29] X. L. Wang,[11] S. Watanuki,[80] E. Widmann,[74] E. Won,[40] H. Ye,[9] J. Yelton,[10] J. H. Yin,[29] C. Z. Yuan,[29] Y. Yusa,[63] Z. P. Zhang,[71] V. Zhilich,[5,64] V. Zhukova,[44,53] and V. Zhulanov[5,64]

(The Belle Collaboration)

[1] *University of the Basque Country UPV/EHU, 48080 Bilbao*
[2] *Beihang University, Beijing 100191*
[3] *University of Bonn, 53115 Bonn*
[4] *Brookhaven National Laboratory, Upton, New York 11973*
[5] *Budker Institute of Nuclear Physics SB RAS, Novosibirsk 630090*
[6] *Faculty of Mathematics and Physics, Charles University, 121 16 Prague*
[7] *Chonnam National University, Kwangju 660-701*
[8] *University of Cincinnati, Cincinnati, Ohio 45221*
[9] *Deutsches Elektronen–Synchrotron, 22607 Hamburg*
[10] *University of Florida, Gainesville, Florida 32611*
[11] *Key Laboratory of Nuclear Physics and Ion-beam Application (MOE) and Institute of Modern Physics, Fudan University, Shanghai 200443*
[12] *Justus-Liebig-Universität Gießen, 35392 Gießen*
[13] *Gifu University, Gifu 501-1193*
[14] *II. Physikalisches Institut, Georg-August-Universität Göttingen, 37073 Göttingen*
[15] *SOKENDAI (The Graduate University for Advanced Studies), Hayama 240-0193*
[16] *Gyeongsang National University, Chinju 660-701*
[17] *Hanyang University, Seoul 133-791*
[18] *University of Hawaii, Honolulu, Hawaii 96822*
[19] *High Energy Accelerator Research Organization (KEK), Tsukuba 305-0801*
[20] *J-PARC Branch, KEK Theory Center, High Energy Accelerator Research Organization (KEK), Tsukuba 305-0801*
[21] *Forschungszentrum Jülich, 52425 Jülich*
[22] *IKERBASQUE, Basque Foundation for Science, 48013 Bilbao*
[23] *Indian Institute of Science Education and Research Mohali, SAS Nagar, 140306*
[24] *Indian Institute of Technology Bhubaneswar, Satya Nagar 751007*
[25] *Indian Institute of Technology Guwahati, Assam 781039*
[26] *Indian Institute of Technology Hyderabad, Telangana 502285*
[27] *Indian Institute of Technology Madras, Chennai 600036*
[28] *Indiana University, Bloomington, Indiana 47408*
[29] *Institute of High Energy Physics, Chinese Academy of Sciences, Beijing 100049*
[30] *Institute of High Energy Physics, Vienna 1050*

[31]*INFN - Sezione di Napoli, 80126 Napoli*
[32]*INFN - Sezione di Torino, 10125 Torino*
[33]*Advanced Science Research Center, Japan Atomic Energy Agency, Naka 319-1195*
[34]*J. Stefan Institute, 1000 Ljubljana*
[35]*Kanagawa University, Yokohama 221-8686*
[36]*Institut für Experimentelle Kernphysik, Karlsruher Institut für Technologie, 76131 Karlsruhe*
[37]*King Abdulaziz City for Science and Technology, Riyadh 11442*
[38]*Department of Physics, Faculty of Science, King Abdulaziz University, Jeddah 21589*
[39]*Korea Institute of Science and Technology Information, Daejeon 305-806*
[40]*Korea University, Seoul 136-713*
[41]*Kyungpook National University, Daegu 702-701*
[42]*LAL, Univ. Paris-Sud, CNRS/IN2P3, Université Paris-Saclay, Orsay*
[43]*École Polytechnique Fédérale de Lausanne (EPFL), Lausanne 1015*
[44]*P.N. Lebedev Physical Institute of the Russian Academy of Sciences, Moscow 119991*
[45]*Faculty of Mathematics and Physics, University of Ljubljana, 1000 Ljubljana*
[46]*Ludwig Maximilians University, 80539 Munich*
[47]*Luther College, Decorah, Iowa 52101*
[48]*University of Malaya, 50603 Kuala Lumpur*
[49]*University of Maribor, 2000 Maribor*
[50]*Max-Planck-Institut für Physik, 80805 München*
[51]*School of Physics, University of Melbourne, Victoria 3010*
[52]*University of Mississippi, University, Mississippi 38677*
[53]*Moscow Physical Engineering Institute, Moscow 115409*
[54]*Moscow Institute of Physics and Technology, Moscow Region 141700*
[55]*Graduate School of Science, Nagoya University, Nagoya 464-8602*
[56]*Kobayashi-Maskawa Institute, Nagoya University, Nagoya 464-8602*
[57]*Università di Napoli Federico II, 80055 Napoli*
[58]*National Central University, Chung-li 32054*
[59]*National United University, Miao Li 36003*
[60]*Department of Physics, National Taiwan University, Taipei 10617*
[61]*H. Niewodniczanski Institute of Nuclear Physics, Krakow 31-342*
[62]*Nippon Dental University, Niigata 951-8580*
[63]*Niigata University, Niigata 950-2181*
[64]*Novosibirsk State University, Novosibirsk 630090*
[65]*Osaka City University, Osaka 558-8585*
[66]*Pacific Northwest National Laboratory, Richland, Washington 99352*
[67]*Panjab University, Chandigarh 160014*
[68]*Peking University, Beijing 100871*
[69]*University of Pittsburgh, Pittsburgh, Pennsylvania 15260*
[70]*Theoretical Research Division, Nishina Center, RIKEN, Saitama 351-0198*
[71]*University of Science and Technology of China, Hefei 230026*
[72]*Showa Pharmaceutical University, Tokyo 194-8543*
[73]*Soongsil University, Seoul 156-743*
[74]*Stefan Meyer Institute for Subatomic Physics, Vienna 1090*
[75]*Sungkyunkwan University, Suwon 440-746*
[76]*School of Physics, University of Sydney, New South Wales 2006*
[77]*Department of Physics, Faculty of Science, University of Tabuk, Tabuk 71451*
[78]*Tata Institute of Fundamental Research, Mumbai 400005*
[79]*Department of Physics, Technische Universität München, 85748 Garching*
[80]*Department of Physics, Tohoku University, Sendai 980-8578*
[81]*Department of Physics, University of Tokyo, Tokyo 113-0033*
[82]*Tokyo Institute of Technology, Tokyo 152-8550*
[83]*Tokyo Metropolitan University, Tokyo 192-0397*
[84]*Virginia Polytechnic Institute and State University, Blacksburg, Virginia 24061*
[85]*Wayne State University, Detroit, Michigan 48202*
[86]*Yamagata University, Yamagata 990-8560*
[87]*Yonsei University, Seoul 120-749*

We report evidence for the charged charmed-strange baryon $\Xi_c(2930)$ with a signal significance of 3.9σ. The charged $\Xi_c(2930)$ is found in its decay to $K^0_S\Lambda_c$ in the substructure of $B^0 \to K^0_S\Lambda_c^+\bar{\Lambda}_c^-$ decays. The measured mass and width are $[2942.3 \pm 4.4(\text{stat.}) \pm 1.6(\text{syst.})]$ MeV/c^2 and $[14.8 \pm 8.8(\text{stat.}) \pm 7.1(\text{syst.})]$ MeV, respectively, and the product branching fraction is $\mathcal{B}(B^0 \to \Xi_c^+(2930)\bar{\Lambda}_c^-)\mathcal{B}(\Xi_c^+(2930) \to K^0\Lambda_c^+) = [2.28 \pm 0.49(\text{stat.}) \pm 0.29(\text{syst.})] \times 10^{-4}$. We also measure $\mathcal{B}(B^0 \to K^0\Lambda_c^+\bar{\Lambda}_c^-) = [3.84 \pm 0.73(\text{stat.}) \pm 0.48(\text{syst.})] \times 10^{-4}$ with greater precision than previous

experiments, and present the results of a search for the charmonium-like state $Y(4660)$ and its spin partner, Y_η, in the $\Lambda_c^+\bar{\Lambda}_c^-$ invariant mass spectrum. No clear signals of the $Y(4660)$ or Y_η are observed and the 90% credibility level (C.L.) upper limits on their production rates are determined. These measurements are obtained from a sample of $(772\pm11)\times10^6 B\bar{B}$ pairs collected at the $\Upsilon(4S)$ resonance by the Belle detector at the KEKB asymmetric energy electron-positron collider.

PACS numbers: 13.25.Hw, 14.20.Lq, 14.40.Rt

The study of the excited states of charmed and bottom baryons is important as they offer an excellent laboratory for testing the heavy-quark symmetry of the c and b quarks and the chiral symmetry of the light quarks. At present, the particle data group (PDG) lists ten charmed-strange baryons [1]. Among these, $\Xi_c(2930)$ and $\Xi_c(3123)$ are relatively less established and evidence for them is poor [1]. For most of these excited Ξ_c states the spins and parities have not been determined by experiments due to limited statistics.

Theoretically, the mass spectrum of excited charmed baryons has been computed in many models, including quark potential models [2–6], the relativistic flux tube model [7, 8], the coupled channel model [9], the Quantum Chromodynamics (QCD) sum rule [10–14], Regge phenomenology [15], the constituent quark model [16, 17], and lattice QCD [18, 19]. The strong decays of excited Ξ_c baryons have also been studied in many models [20–26]. In these models, some possible J^P assignments of these excited Ξ_c have been performed. While many new excited charmed baryons have been discovered in experiments in recent years, and there has been much theoretical work devoted to study the nature of charmed baryon internal structure and quark organization, further effort (and cooperation) from both experimentalists and theorists is needed to make progress in this area.

Very recently, Belle reported the first observation of the $\Xi_c(2930)^0$ charmed-strange baryon with a significance greater than 5σ by study of the substructure in $B^- \to K^-\Lambda_c^+\bar{\Lambda}_c^-$ decays [27]. The measured mass and width of the $\Xi_c(2930)^0$ were found to be $[2928.9\pm3.0(\text{stat.})^{+0.9}_{-12.0}(\text{syst.})]$ MeV/c^2 and $[19.5\pm8.4(\text{stat.})^{+5.9}_{-7.9}(\text{syst.})]$ MeV, respectively. As the isospin of the Ξ_c state is 1/2 and the neutral $\Xi_c(2930)$ has been found, it is natural to search for the charged partner in the substructure in $B^0\to K^0\Lambda_c^+\bar{\Lambda}_c^-$ decays [28].

BaBar and Belle have previously studied $B^0 \to K^0\Lambda_c^+\bar{\Lambda}_c^-$ decays using data samples of 230×10^6 and 386×10^6 $B\bar{B}$ pairs, and found signals of 1.4σ and 6.6σ significances, respectively [29, 30]. Neither experiment searched for possible intermediate states in the $K_S^0\Lambda_c$ system. The full Belle data sample of $(772\pm11)\times10^6 B\bar{B}$ pairs permits an improved study of $B^0\to K^0\Lambda_c^+\bar{\Lambda}_c^-$ and a search for the charged $\Xi_c(2930)$ in the decay mode $K^0\Lambda_c$.

The $\Lambda_c^+\bar{\Lambda}_c^-$ system is interesting because (1) Belle has observed the $Y(4630)$ in the initial state radiation (ISR) process $e^+e^-\to\gamma_{\rm ISR}\Lambda_c^+\bar{\Lambda}_c^-$ and measured a mass and width of $[4634^{+8}_{-7}(\text{stat.})^{+5}_{-8}(\text{syst.})]$ MeV/c^2 and $[92^{+40}_{-24}(\text{stat.})^{+10}_{-21}(\text{syst.})]$ MeV, respectively [31]; (2) Belle has also observed the $Y(4660)$ in $e^+e^-\to\gamma_{\rm ISR}\pi^+\pi^-\psi'$ with a measured mass and width of $[4652\pm10(\text{stat.})\pm8(\text{syst.})]$ MeV/c^2 and $[68\pm11(\text{stat.})\pm1(\text{syst.})]$ MeV, respectively [32, 33]. As the masses and widths of the $Y(4630)$ and $Y(4660)$ are close to each other, many theoretical explanations assume they are the same state [34–36]. In Refs. [37, 38], the authors predicted a $Y(4660)$ spin partner—a $f_0(980)\eta_c(2S)$ bound state denoted the Y_η—with a mass and width of (4613 ± 4) MeV/c^2 and around 30 MeV, respectively, with the assumption that the $Y(4660)$ is an $f_0(980)\psi'$ bound state [36, 38]. Belle has searched for these states in the substructure of $B^-\to K^-\Lambda_c^+\bar{\Lambda}_c^-$ decays, and no clear signals were observed [27]. The corresponding B^0 decay mode can also be used to study the $\Lambda_c^+\bar{\Lambda}_c^-$ invariant mass.

In this letter, we perform an updated measurement of $B^0\to K^0\Lambda_c^+\bar{\Lambda}_c^-$ and find the $\Xi_c(2930)^\pm$ signal, which we denote as $\Xi_c(2930)^+$ and $\bar{\Xi}_c(2930)^-$ hereafter, with a significance of 3.9σ. This analysis is based on the full data sample collected at the $\Upsilon(4S)$ resonance by the Belle detector [39] at the KEKB asymmetric energy electron-positron collider [40].

The Belle detector is a large solid angle magnetic spectrometer that consists of a silicon vertex detector, a 50-layer central drift chamber (CDC), an array of aerogel threshold Cherenkov counters (ACC), a barrel-like arrangement of time-of-flight scintillation counters (TOF), and an electromagnetic calorimeter comprised of CsI(Tl) crystals located inside a superconducting solenoid coil that provides a 1.5 T magnetic field. An iron flux-return yoke located outside the coil is instrumented to detect K_L^0 mesons and to identify muons. A detailed description of the Belle detector can be found in Ref. [39]. Simulated signal events with B meson decays are generated using EvtGen [41], while the inclusive decays are generated via PYTHIA [42]. These events are processed by a detector simulation based on GEANT3 [43]. Inclusive Monte Carlo (MC) samples of $\Upsilon(4S)\to B\bar{B}$ ($B=B^+$ or B^0) and $e^+e^-\to q\bar{q}$ ($q=u,\ d,\ s,\ c$) events at $\sqrt{s}=10.58$ GeV, corresponding to more than 5 times the integrated luminosity of the data, are used to check the backgrounds.

In our analysis of $B^0\to K^0\Lambda_c^+\bar{\Lambda}_c^-$, the K^0 is reconstructed via its decay $K_S^0\to\pi^+\pi^-$, and Λ_c^+ candidates are reconstructed in the $\Lambda_c^+\to pK^-\pi^+$, pK_S^0, and $\Lambda\pi^+(\to p\pi^-\pi^+)$ decay channels. A Λ_c^+ and $\bar{\Lambda}_c^-$, together with a K_S^0, are combined to reconstruct a B candidate,

with at least one required to have been reconstructed via the $pK^-\pi^+$ or $\bar{p}K^+\pi^-$ decay process.

For well reconstructed charged tracks, except for those from $\Lambda \to p\pi^-$ and $K^0_S \to \pi^+\pi^-$ decays, the impact parameters perpendicular to and along the beam direction with respect to the nominal interaction point are required to be less than 0.5 cm and 4 cm, respectively, and the transverse momentum in the laboratory frame is required to be larger than 0.1 GeV/c. The information from different detector subsystems including specific ionization in the CDC, time measurements in the TOF and response of the ACC is combined to form the likelihood $\mathcal{L}_i$ of the track for particle species i, where $i = \pi$, K or p [44]. Except for the charged tracks from $\Lambda \to p\pi^-$ and $K^0_S \to \pi^+\pi^-$ decays, tracks with a likelihood ratio $\mathcal{R}^\pi_K = \mathcal{L}_K/(\mathcal{L}_K + \mathcal{L}_\pi) > 0.6$ are identified as kaons, while tracks with $\mathcal{R}^\pi_K < 0.4$ are treated as pions. The kaon (pion) identification efficiency is about 94% (97%), while 5% (3%) of the kaons (pions) are misidentified as pions (kaons) with the selection criteria above. For proton identification, a track with $\mathcal{R}^\pi_{p/\bar{p}} = \mathcal{L}_{p/\bar{p}}/(\mathcal{L}_{p/\bar{p}} + \mathcal{L}_\pi) > 0.6$ and $\mathcal{R}^K_{p/\bar{p}} = \mathcal{L}_{p/\bar{p}}/(\mathcal{L}_{p/\bar{p}} + \mathcal{L}_K) > 0.6$ is identified as a proton/anti-proton with an efficiency of about 98%; fewer than 1% of the pions/kaons are misidentified as protons/anti-protons.

The K^0_S candidates are reconstructed from pairs of oppositely-charged tracks, treated as pions, and identified by a multivariate analysis with a neural network [45] based on two sets of input variables [46]. Candidate Λ baryons are reconstructed in the decay $\Lambda \to p\pi^-$ and selected if the $p\pi^-$ invariant mass is within 5 MeV/c^2 (5σ) of the Λ nominal mass [1].

A vertex fit to the B candidates is performed and the one with the minimum $\chi^2_{\rm vertex}/n.d.f.$ from the vertex fit is selected as the signal B candidate if there is more than one B candidate in an event, where $n.d.f.$ is the number of degrees of freedom of the vertex fit. The $\chi^2_{\rm vertex}/n.d.f. < 15$ is required, providing a selection efficiency above 96%. As the continuum background level is very low, further continuum suppression is not necessary.

The B candidates are identified using the beam-energy constrained mass $M_{\rm bc}$ and the mass difference ΔM_B. The beam-energy constrained mass is defined as $M_{\rm bc} \equiv \sqrt{E^2_{\rm beam}/c^2 - (\sum \vec{p}_i)^2}/c$, where $E_{\rm beam}$ is the beam energy and $\vec{p}_i$ are the three-momenta of the B-meson decay products, all defined in the center-of-mass system (CMS) of the e^+e^- collision. The mass difference is defined as $\Delta M_B \equiv M_B - m_B$, where M_B is the invariant mass of the B candidate and m_B is the nominal B-meson mass [1]. The B signal region is defined as $|\Delta M_B| < 0.018$ GeV/c^2 and $M_{\rm bc} > 5.272$ GeV/c^2 ($\sim 2.5\sigma$) which is shown as the central box in the distribution of ΔM_B versus $M_{\rm bc}$ in Fig 1.

The scatter plot of $M_{\bar{\Lambda}_c^-}$ versus $M_{\Lambda_c^+}$ is shown in the left panel of Fig. 1 for the selected $B^0 \to K^0_S\Lambda_c^+\bar{\Lambda}_c^-$ data candidates in the B signal region, and clear Λ_c^+ and $\bar{\Lambda}_c^-$ signals are observed. According to the signal MC simulation, the mass resolution of Λ_c candidates is almost independent of the Λ_c decay mode. The Λ_c signal region is defined as $|M_{\Lambda_c} - m_{\Lambda_c}| < 12$ MeV/c^2 ($\sim 2.5\sigma$) for all Λ_c decay modes illustrated by the central green box in the Fig. 1 (left panel), where m_{Λ_c} is the nominal mass of the Λ_c baryon [1]. To estimate the non-Λ_c backgrounds, we define the Λ_c^+ and $\bar{\Lambda}_c^-$ mass sidebands as half of the total number of events in the four red sideband regions minus one quarter of the total number of events in the four blue sideband regions as shown in Fig. 1 (left panel).

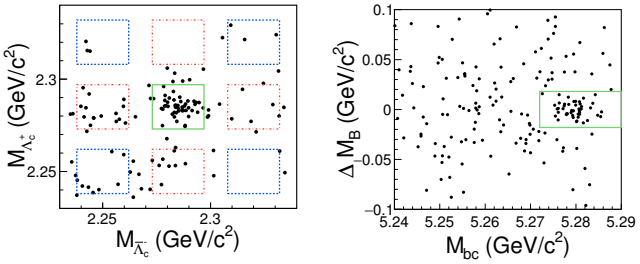


FIG. 1: Signal-enhanced distributions of $M(\bar{\Lambda}_c^-)$ versus $M(\Lambda_c^+)$ (left panel) and of ΔM_B versus $M_{\rm bc}$ (right panel) from the selected $B^0 \to K^0\Lambda_c^+\bar{\Lambda}_c^-$ candidates, summing over all three reconstructed Λ_c decay modes. Each panel shows the events falling in the solid green signal region of the other panel. The dashed red and blue boxes in the left panel show the Λ_c sideband regions described in the text, which are used for the estimation of the non-Λ_c background.

To extract the $B^0 \to K^0_S\Lambda_c^+\bar{\Lambda}_c^-$ signal yields, we perform an unbinned two-dimensional (2D) simultaneous extended maximum likelihood fit to the ΔM_B versus $M_{\rm bc}$ distributions for the three reconstructed Λ_c decay modes. A Gaussian function for the signal shape plus an ARGUS function [47] for the background are used to fit the $M_{\rm bc}$ distribution, while the sum of a double-Gaussian function for the signal plus a first-order polynomial for the background are used to fit the ΔM_B distribution. Due to limited statistics, all the parameters of the Gaussian functions are fixed to the values from the fits to the individual MC signal distributions, and the relative signal yields among the three final states are fixed according to the relative branching fraction between the final states and the detection acceptance and efficiency of the intermediate states.

The projections of $M_{\rm bc}$ and ΔM_B summed over the three reconstructed Λ_c decay modes in Λ_c signal region, together with the fitted results, are shown in Fig. 2. There are 34.9 ± 6.6 signal events with a statistical signal significance above 8.3σ, and we extract the branching fraction of $\mathcal{B}(B^0 \to K^0\Lambda_c^+\bar{\Lambda}_c^-) = [3.84 \pm 0.73(\text{stat.})] \times 10^{-4}$.

After applying all selection criteria above, the Dalitz

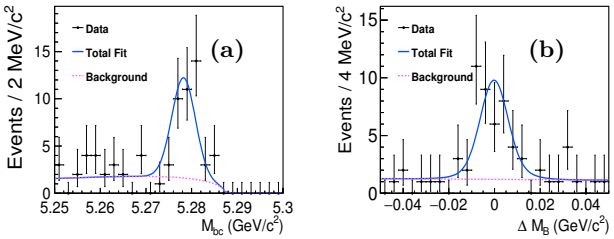


FIG. 2: The Λ_c-signal-enhanced distributions of (a) $M_{\rm bc}$ in the ΔM_B signal region and (b) ΔM_B in the $M_{\rm bc}$ signal region for $B^0 \to K^0_S\Lambda_c^+\bar{\Lambda}_c^-$, combining three exclusive final states. The dots with error bars are data, the solid blue curves are the best-fit projections to the distributions, and the dashed magenta lines are the fitted backgrounds.

distribution of the $M^2_{K^0_S\Lambda_c^+}$ versus $M^2_{K^0_S\bar{\Lambda}_c^-}$ is shown in Fig. 3. Enhancements can be seen in the vertical and horizontal bands corresponding to $M(K^0_S\Lambda_c) \sim 2.93$ GeV/c^2, while no signal band is apparent in the $M(\Lambda_c^+\bar{\Lambda}_c^-)$ diagonal direction.

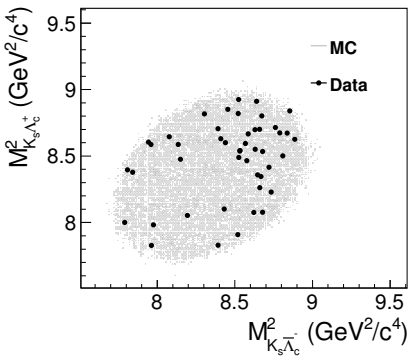


FIG. 3: Dalitz distribution of reconstructed $B^0 \to K^0_S\Lambda_c^+\bar{\Lambda}_c^-$ candidates in the B signal region. The black dots are data; the shaded region is the MC simulated phase-space distribution.

The $M_{\Lambda_c^+\bar{\Lambda}_c^-}$ spectrum is shown in Fig. 4, where the shaded cyan histogram is from the normalized Λ_c^+ and $\bar{\Lambda}_c^-$ mass sidebands. No signals of Y_η or $Y(4660)$ are evident. An unbinned extended maximum likelihood fit is applied to the $\Lambda_c^+\bar{\Lambda}_c^-$ mass spectrum to extract the signal yields of the Y_η and $Y(4660)$ in B decays separately. In the fit, the signal shape of the Y_η or $Y(4660)$ is obtained from MC simulation directly, with the input parameters $M_{Y_\eta} = 4616$ MeV/c^2 and $\Gamma_{Y_\eta} = 30$ MeV for Y_η [36], and $M_{Y(4660)} = 4643$ MeV/c^2 and $\Gamma_{Y(4660)} = 72$ MeV for $Y(4660)$ [1]; a third-order polynomial is used to describe all other contributions. The fit results are shown in Figs. 4(a) and (b) for the Y_η and $Y(4660)$, respectively. From the fits, we obtain (18.1 ± 8.4) Y_η and (28.1 ± 11.1) $Y(4660)$ signal events each with a signal statistical significance of 2.3σ.

As the statistical signal significance of each Y state is less than 3σ, assuming that the number of signal events follows a Poisson distribution with a uniform prior probability density function, 90% C.L. Bayesian upper limits on $\mathcal{B}(B^0 \to K^0 Y)\mathcal{B}(Y \to \Lambda_c^+\bar{\Lambda}_c^-)$ are determined to be 3.2×10^{-4} and 4.9×10^{-4} for $Y = Y_\eta$ and $Y(4660)$, respectively, by solving the equation $\int_0^{\mathcal{B}^{\rm up}} \mathcal{L}(\mathcal{B})d\mathcal{B} / \int_0^{+\infty} \mathcal{L}(\mathcal{B})d\mathcal{B} = 0.9$, where $\mathcal{B} = \frac{n_Y}{\varepsilon^Y_{\rm all} N_{B^0\bar{B}^0} \mathcal{B}(\Lambda_c^+ \to pK^-\pi^+)^2}$ is the assumed product branching fraction; $\mathcal{L}(\mathcal{B})$ is the corresponding maximized likelihood of the data; n_Y is the number of Y signal events; and $\varepsilon^Y_{\rm all} = \sum \varepsilon^Y_i \times \Gamma_i/\Gamma(pK^-\pi^+)$ (ε^Y_i being the detection efficiency from MC simulation for mode i). To take the systematic uncertainty into account, the above likelihood is convolved with a Gaussian function whose width equals the total systematic uncertainty discussed below.

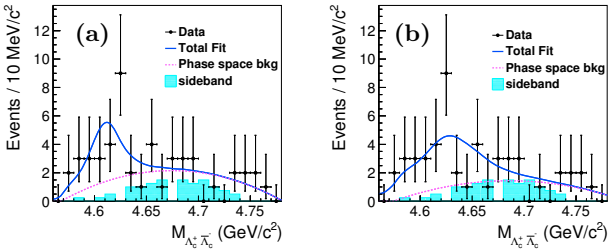


FIG. 4: The $\Lambda_c^+\bar{\Lambda}_c^-$ invariant mass spectra in data with (a) Y_η and (b) Y(4660) signals included in the fits. The solid blue lines are the best fits and the dotted magenta lines represent the backgrounds. The shaded cyan histograms are from the normalized Λ_c^+ and $\bar{\Lambda}_c^-$ mass sidebands.

The sum of the projections of $M_{K^0_S\Lambda_c^+}$ and $M_{K^0_S\bar{\Lambda}_c^-}$ mass spectra, denoted $M_{K^0_S\Lambda_c}$, is shown in Fig. 5. The shaded histogram is from the normalized Λ_c^+ and $\bar{\Lambda}_c^-$ mass sidebands, which is consistent with the contributions from normalized $e^+e^- \to q\bar{q}$ and $\Upsilon(4S) \to B\bar{B}$ generic MC samples. Therefore, the estimate from the normalized Λ_c^+ and $\bar{\Lambda}_c^-$ mass sidebands is taken to represent the total background, neglecting the small possible contribution of background with real Λ_c^+ and $\bar{\Lambda}_c^-$. A clear $\Xi_c(2930)^\pm$ signal is found. No structure is seen in the Λ_c^+ and $\bar{\Lambda}_c^-$ mass sidebands.

An unbinned simultaneous extended maximum likelihood fit is performed to the $K^0_S\Lambda_c$ invariant mass spectra for the total selected signal candidates and the Λ_c^+ and $\bar{\Lambda}_c^-$ mass sidebands. The following components are included in the fit: an S-wave Breit-Wigner (BW) function convolved with a Gaussian function with the phase space factor and efficiency curve included (the mass resolution of the Gaussian function being fixed to 5.36 MeV/c^2 from the signal MC simulation) is taken as the $\Xi_c(2930)^\pm$ signal shape; a broader structure obtained by MC simulation is used to represent the reflection of the $\Xi_c(2930)^\pm$; direct three-body $B^0 \to K^0_S\Lambda_c^+\bar{\Lambda}_c^-$ decays are modeled by

the MC-simulated shape distributed uniformly in phase space; a second-order polynomial is used to represent the Λ_c^+ and $\bar{\Lambda}_c^-$ mass-sideband distribution, which is normalized to represent the total background in the signal events in the fit. In the above fit, the signal yields of the $\Xi_c(2930)^\pm$ and the corresponding reflection are constrained to be the same.

The fit results are shown in Fig. 5, where the solid blue line is the best fit, and the solid violet line is the total non-$\Xi_c(2930)^\pm$ backgrounds including the fitted phase space, the reflection of the $\Xi_c(2930)^\pm$, and the fitted sideband shape. The yields of the $\Xi_c(2930)^\pm$ signal and the phase-space contribution are $N_{\Xi_c(2930)} = 21.2 \pm 4.6$ and $N_{phsp} = 18.3 \pm 4.6$. The fitted mass and width are $M_{\Xi_c(2930)^+} = [2942.3 \pm 4.4(\text{stat.})]$ MeV/c^2 and $\Gamma_{\Xi_c(2930)^+} = [14.8 \pm 8.8(\text{stat.})]$ MeV, respectively, where the correction of 2.8 MeV/c^2 has been applied on $\Xi_c(2930)^\pm$ mass, determined using the input and output mass difference by MC simulation. The statistical significance of the $\Xi_c(2930)^\pm$ signal is 4.1σ, calculated from the difference of the logarithmic likelihoods [48], $-2\ln(\mathcal{L}_0/\mathcal{L}_{\max}) = 23.1$, where $\mathcal{L}_0$ and $\mathcal{L}_{\max}$ are the maximized likelihoods without and with a signal component, respectively, taking into account the difference in the number of degrees of freedom (Δn.d.f. = 3). The signal significance remains at 3.9σ when convolving the likelihood profile with a Gaussian function of width that equals the total systematic uncertainty from detection efficiency, fitting procedure, and intermediate states' branching fractions. Alternative fits to the $K_S^0\Lambda_c$ mass spectra are performed (a) using a first-order or third-order polynomial as the background shape; (b) changing the $\Xi_c(2930)^\pm$ mass resolution by $\pm 10\%$; and (c) using an energy-dependent BW function as the $\Xi_c(2930)^\pm$ signal shape. The $\Xi_c(2930)^\pm$ signal significance is larger than 3.5σ in all cases.

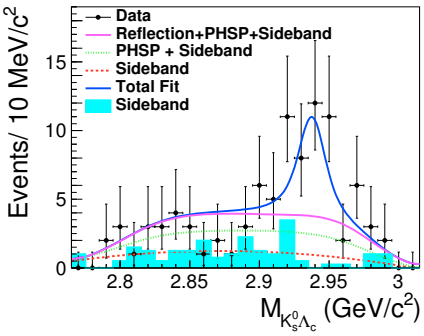


FIG. 5: The $M_{K_S^0\Lambda_c}$ distribution of the selected data candidates, with fit results superimposed. Dots with error bars are the data, the solid blue line is the best fit, the solid violet line is the total non-$\Xi_c(2930)^\pm$ backgrounds, the dotted green line is the fitted phase space and sideband shape, the dotted red line is the fitted sideband shape, the shaded cyan histogram is from the normalized Λ_c^+ and $\bar{\Lambda}_c^-$ mass sidebands

.

The product of $\mathcal{B}(B^0 \to \Xi_c(2930)^+\bar{\Lambda}_c^-)$ and $\mathcal{B}(\Xi_c(2930)^+ \to K^0\Lambda_c^+)$ is $[(2.28 \pm 0.49(\text{stat.})] \times 10^{-4}$ calculated as $N_{\Xi_c(2930)^+}/(\varepsilon_{all}^{\Xi_c(2930)^+} N_{B^0\bar{B}^0}\mathcal{B}(\Lambda_c^+ \to pK^-\pi^+)^2)$, where $N_{\Xi_c(2930)^+}$ is the fitted $\Xi_c(2930)^\pm$ signal yield; $N_{B^0\bar{B}^0} = N_{\Upsilon(4S)}\mathcal{B}(\Upsilon(4S) \to B^0\bar{B}^0)$ with $N_{\Upsilon(4S)}$ being the number of accumulated $\Upsilon(4S)$ events and $\mathcal{B}(\Upsilon(4S) \to B^0\bar{B}^0) = 0.486 \pm 0.006$ [1]; for $\mathcal{B}(\Lambda_c^+ \to pK^-\pi^+)$, we use the world-average value, $(6.35 \pm 0.33)\%$ [1]. The efficiency $\varepsilon_{all}^{\Xi_c(2930)^+}$, combined for all three Λ_c decay modes, is obtained by $\varepsilon_{all}^{\Xi_c(2930)^+} = \Sigma\varepsilon_i^{\Xi_c(2930)^+}\Gamma_i/\Gamma(pK^-\pi^+)$, where i is the index for Λ_c decay-mode, $\varepsilon_i^{\Xi_c(2930)^+}$ is the detection efficiency for the i-the mode obtained by fitting $M_{K_S^0\Lambda_c}$ spectrum from signal MC with a $\Xi_c(2930)^\pm$ intermediate state, and Γ_i is the partial decay width of $\Lambda_c^+ \to pK^-\pi^+$, pK_S^0, and $\Lambda\pi^-$, for which we use the world-average values [1]. Here, $\mathcal{B}(K_S^0 \to \pi^+\pi^-)$ or $\mathcal{B}(\Lambda \to p\pi^-)$ is included in Γ_i for the final states with a K_S^0 or a Λ.

The systematic uncertainties in the branching fraction measurements are listed below. The uncertainties related to detection efficiency (DER) include those for tracking efficiency (0.35%/track), particle identification efficiency (1.0%/kaon, 0.9%/pion, 3.7%/proton and 3.4%/anti-proton), as well as Λ (3.0%) and K_S^0 (2.3%) selection efficiencies. Assuming all the above systematic uncertainty sources are independent, the DER uncertainties are summed in quadrature for each decay mode, yielding 5.8–8.6%, depending on the mode. For the four branching fraction measurements, the final DER uncertainties are summed in quadrature over the three Λ_c decay modes using weight factors equal to the product of the total efficiency and the Λ_c partial decay width. Systematic uncertainties associated with the fitting procedure are estimated by changing the order of the background polynomial, the range of the fit, and the values of the masses and widths of the Y_η and $Y(4660)$ by $\pm 1\sigma$, and by enlarging the mass resolution by 10% with the deviations from nominal in the fitted results taken as systematic uncertainties. Uncertainties for $\mathcal{B}(\Lambda_c^+ \to pK^-\pi^+)$ and $\Gamma_i/\Gamma(pK^-\pi^+)$ are taken from Ref. [1]. The final uncertainties on the Λ_c partial decay widths are summed in quadrature over the three modes weighted by the detection efficiency. The world average of $\mathcal{B}(\Upsilon(4S) \to B^0\bar{B}^0)$ is $(48.6 \pm 0.6)\%$ [1], which corresponds to a systematic uncertainty of 1.23%. The systematic uncertainty on $N_{\Upsilon(4S)}$ is 1.37%. The total systematic uncertainties are obtained by adding the uncertainties from all sources in quadrature, and are listed in Table I.

The sources of systematic uncertainties of $\Xi_c(2930)^\pm$ mass and width measurements are calculated by the following method. Half of the correction due to the input and output difference on the $\Xi_c(2930)^\pm$ mass determined from MC simulation is conservatively taken as a system-

TABLE I: Relative systematic uncertainties (%) in the branching fraction measurements. Here, $\mathcal{B}_1 \equiv \mathcal{B}(B^0 \to K^0\Lambda_c^+\bar{\Lambda}_c^-)$, $\mathcal{B}_2 \equiv \mathcal{B}(B^0 \to \Xi_c(2930)^+\bar{\Lambda}_c^-)\mathcal{B}(\Xi_c(2930)^+ \to K^-\Lambda_c^+)$, $\mathcal{B}_3 \equiv \mathcal{B}(B^0 \to K^0 Y_\eta)\mathcal{B}(Y_\eta \to \Lambda_c^+\bar{\Lambda}_c^-)$, and $\mathcal{B}_4 \equiv \mathcal{B}(B^0 \to K^0 Y(4660))\mathcal{B}(Y(4660) \to \Lambda_c^+\bar{\Lambda}_c^-)$.

Branching fraction	DER	Fit	Λ_c decays	$N_{B^0\bar{B}^0}$	Sum
$\mathcal{B}_1$	5.28	4.20	10.5	1.82	12.6
$\mathcal{B}_2$	5.31	5.10	10.5	1.82	12.9
$\mathcal{B}_3$	5.28	10.1	10.5	1.82	15.6
$\mathcal{B}_4$	5.27	25.3	10.5	1.82	27.9

atic uncertainty. By enlarging the mass resolution by 10%, the difference in the measured $\Xi_c(2930)$ width is 0.9 MeV, and this is taken as a systematic uncertainty. By changing the background shape, the differences of 0.5 MeV/c^2 and 1.3 MeV in the measured $\Xi_c(2930)^\pm$ mass and width, respectively, are taken as systematic uncertainties.

The signal-parametrization systematic uncertainty is estimated by replacing the constant total width with a mass-dependent width of $\Gamma_t = \Gamma_t^0 \times \Phi(M_{K_S^0\Lambda_c})/\Phi(M_{\Xi_c(2930)})$, where Γ_t^0 is the width of the resonance, $\Phi(M_{K_S^0\Lambda_c}) = P/M_{K_S^0\Lambda_c}$ is the phase space factor for an S-wave two-body system (P is the K_S^0 momentum in the $K_S^0\Lambda_c$ CMS) and $M_{\Xi_c(2930)}$ is the $K_S^0\Lambda_c$ invariant mass fixed at the $\Xi_c(2930)^\pm$ nominal fitted mass. The differences in the measured $\Xi_c(2930)^\pm$ mass and width are 0.5 MeV/c^2 and 6.9 MeV, respectively, which are taken as the systematic uncertainties. Assuming all the sources are independent, we add them in quadrature to obtain the total systematic uncertainties on the $\Xi_c(2930)^\pm$ mass and width of 1.6 MeV/c^2 and 7.1 MeV, respectively.

In summary, using $(772 \pm 11) \times 10^6$ $B\bar{B}$ pairs, we perform an updated analysis of $B^0 \to K^0\Lambda_c^+\bar{\Lambda}_c^-$ decays. There is evidence at the 3.9σ level of the charmed baryon state $\Xi_c(2930)^\pm$ in the $K_S^0\Lambda_c$ mass spectrum. The measured mass and width are $M_{\Xi_c(2930)^+} = [2942.3 \pm 4.4(\text{stat.}) \pm 1.6(\text{syst.})]$ MeV/c^2 and $\Gamma_{\Xi_c(2930)^+} = [14.8 \pm 8.8(\text{stat.}) \pm 7.1(\text{syst.})]$ MeV. The mass and width difference between neutral [27] and charged $\Xi_c(2930)$ are $\Delta m = [-13.4 \pm 5.3(\text{stat.})^{+1.8}_{-12.1}(\text{syst.})]$ MeV/c^2 and $\Delta\Gamma = [4.7 \pm 12.2(\text{stat.})^{+9.2}_{-10.6}(\text{syst.})]$ MeV, respectively. The branching fraction is $\mathcal{B}(B^0 \to K^0\Lambda_c^+\bar{\Lambda}_c^-) = [3.84 \pm 0.73(\text{stat.}) \pm 0.48(\text{syst.})] \times 10^{-4}$, which is consistent with the world average value of $(4.3 \pm 2.2) \times 10^{-4}$ [1] but with improved precision. We measure the product branching fraction $\mathcal{B}(B^0 \to \Xi_c(2930)^+\bar{\Lambda}_c^-)\mathcal{B}(\Xi_c(2930)^+ \to K^0\Lambda_c^+) = [2.28 \pm 0.49(\text{stat.}) \pm 0.29(\text{syst.})] \times 10^{-4}$. We do not perform an angular correlation analysis to determine the spin parity of the $\Xi_c(2930)^\pm$ due to the limited statistics. We are not able to identify the nature of $\Xi_c(2930)^\pm$ with the spin parity not determined since there are many theoretical possibilities. We expect this study to be repeated with a much larger data sample to be collected by the Belle II experiment. There are no significant signals seen in the $\Lambda_c^+\bar{\Lambda}_c^-$ mass spectrum. We place 90% C.L. upper limits for the $Y(4660)$ and its theoretically predicted spin partner Y_η of $\mathcal{B}(B^0 \to K^0 Y(4660))\mathcal{B}(Y(4660) \to \Lambda_c^+\bar{\Lambda}_c^-) < 3.2 \times 10^{-4}$ and $\mathcal{B}(B^0 \to K^0 Y_\eta)\mathcal{B}(Y_\eta \to \Lambda_c^+\bar{\Lambda}_c^-) < 4.9 \times 10^{-4}$ [49].

We thank the KEKB group for the excellent operation of the accelerator; the KEK cryogenics group for the efficient operation of the solenoid; and the KEK computer group, the National Institute of Informatics, and the Pacific Northwest National Laboratory (PNNL) Environmental Molecular Sciences Laboratory (EMSL) computing group for valuable computing and Science Information NETwork 5 (SINET5) network support. We acknowledge support from the Ministry of Education, Culture, Sports, Science, and Technology (MEXT) of Japan, the Japan Society for the Promotion of Science (JSPS), and the Tau-Lepton Physics Research Center of Nagoya University; the Australian Research Council; Austrian Science Fund under Grant No. P 26794-N20; the National Natural Science Foundation of China under Contracts No. 11435013, No. 11475187, No. 11521505, No. 11575017, No. 11675166, No. 11705209; No. 11761141009; Key Research Program of Frontier Sciences, Chinese Academy of Sciences (CAS), Grant No. QYZDJ-SSW-SLH011; the CAS Center for Excellence in Particle Physics (CCEPP); Fudan University Grant No. JIH5913023, No. IDH5913011/003, No. JIH5913024, No. IDH5913011/002; the Ministry of Education, Youth and Sports of the Czech Republic under Contract No. LTT17020; the Carl Zeiss Foundation, the Deutsche Forschungsgemeinschaft, the Excellence Cluster Universe, and the VolkswagenStiftung; the Department of Science and Technology of India; the Istituto Nazionale di Fisica Nucleare of Italy; National Research Foundation (NRF) of Korea Grants No. 2014R1A2A2A01005286, No.2015R1A2A2A01003280, No. 2015H1A2A1033649, No. 2016R1D1A1B01010135, No. 2016K1A3A7A09005 603, No. 2016R1D1A1B02012900; Radiation Science Research Institute, Foreign Large-size Research Facility Application Supporting project and the Global Science Experimental Data Hub Center of the Korea Institute of Science and Technology Information; the Polish Ministry of Science and Higher Education and the National Science Center; the Ministry of Education and Science of the Russian Federation and the Russian Foundation for Basic Research; the Slovenian Research Agency; Ikerbasque, Basque Foundation for Science, Basque Government (No. IT956-16) and Ministry of Economy and Competitiveness (MINECO) (Juan de la Cierva), Spain; the Swiss National Science Foundation; the Ministry of Education and the Ministry of Science and Technology of Taiwan; and the United States Department of Energy

and the National Science Foundation.

[1] C. Patrignani *et al.* (Particle Data Group), Chin. Phys. C **40**, 100001 (2016) and 2017 update.

[2] A. Majethiya, B. Patel, and P.C. Vinodkumar, Eur. Phys. J. A **38**, 307 (2008).

[3] S. Migura, D. Merten, B. Metsch, and H. R. Petry, Eur. Phys. J. A **28**, 41 (2006).

[4] H. Garcilazo, J. Vijande, and A. Valcarce, J. Phys. G **34**, 961 (2007).

[5] D. Ebert, R. N. Faustov, and V. O. Galkin, Phys. Lett. B **659**, 612 (2008).

[6] D. Ebert, R. N. Faustov, and V. O. Galkin, Phys. Rev. D **84**, 014025 (2011).

[7] B. Chen, K. W. Wei, and A. Zhang, Eur. Phys. J. A **51**, 82 (2015).

[8] B. Chen, D. X. Wang, and A. Zhang, Chin. Phys. C **33**, 1327 (2009).

[9] O. Romanets, L. Tolos, C. Garcia-Recio, J. Nieves, L. L. Salcedo, and R. G. E. Timmermans, Phys. Rev. D **85**, 114032 (2012).

[10] Z. G. Wang, Eur. Phys. J. A **45**, 267 (2010).

[11] Z. G. Wang, Eur. Phys. J. C **75**, 359 (2015).

[12] D. D. Ye, Z. Zhao, and A. Zhang, Phys. Rev. D **96**, 114009 (2017).

[13] T. M. Aliev, K. Azizi and H. Sundu, arXiv:1803.04002.

[14] H. X. Chen, W. Chen, Q. Mao, A. Hosaka, X. Liu, and S.L. Zhu, Phys. Rev. D **91**, 054034 (2015).

[15] X. H. Guo, K. W. Wei, and X. H. Wu, Phys. Rev. D **78**, 056005 (2008).

[16] K. L. Wang, Y. X. Yao, X. H. Zhong, and Q. Zhao, Phys. Rev. D **96**, 116016 (2017).

[17] B. Chen, K. W. Wei, X. Liu, and T. Matsuki, Eur. Phys. J. C **77**, 154 (2017).

[18] M. Padmanath, R. G. Edwards, N. Mathur, and M. Peardon, arXiv:1311.4806.

[19] M. Padmanath and N. Mathur, arXiv:1508.07168.

[20] B. Chen, X. Liu, and A. Zhang, Phys. Rev. D **95**, 074022 (2017).

[21] H. Y. Cheng and C. K. Chua, Phys. Rev. D **75**, 014006 (2007).

[22] H. Y. Cheng and C. K. Chua, Phys. Rev. D 92, 074014 (2015).

[23] C. Chen, X. L. Chen, X. Liu, W. Z. Deng, and S. L. Zhu, Phys. Rev. D **75**, 094017 (2007).

[24] L. H. Liu, L. Y. Xiao, and X. H. Zhong, Phys. Rev. D **86**, 034024 (2012).

[25] Z. Zhao, D. D. Ye, and A. Zhang, Phys. Rev. D **94**, 114020 (2016).

[26] H. X. Chen, Q. Mao, W. Chen, A. Hosaka, X. Liu, and S. L. Zhu, Phys. Rev. D **95**, 094008 (2017).

[27] Y. B. Li *et al.* (Belle Collaboration), Eur. Phys. J. C **78**, 252 (2018).

[28] Inclusion of charge conjugate states is implicit unless otherwise stated.

[29] B. Aubert *et al.* (BaBar Collaboration), Phys. Rev. D **77**, 031101 (2008).

[30] N. Gabyshev *et al.* (Belle Collaboration), Phys. Rev. Lett. **97**, 202003 (2006).

[31] G. Pakhlova *et al.* (Belle Collaboration), Phys. Rev. Lett. **101**, 172001 (2008).

[32] X. L. Wang *et al.* (Belle Collaboration), Phys. Rev. Lett. **99**, 142002 (2007).

[33] X. L. Wang *et al.* (Belle Collaboration), Phys. Rev. D **91** 112007 (2015).

[34] D. V. Bugg, J. Phys. G **36**, 075002 (2009).

[35] G. Cotugno, R. Faccini, A. D. Polosa, and C. Sabelli, Phys. Rev. Lett. **104**, 132005 (2010).

[36] F. K. Guo, J. Haidenbauer, C. Hanhart, and U. G. Meißner, Phys. Rev. D **82**, 094008 (2010).

[37] F. K. Guo, C. Hanhart, and U. G. Meißner, Phys. Lett. B **665**, 26 (2008).

[38] F. K. Guo, C. Hanhart, and U. G. Meißner, Phys. Rev. Lett. **102**, 242004 (2009).

[39] A. Abashian *et al.* (Belle Collaboration), Nucl. Instrum. Methods Phys. Res., Sect. A **479**, 117 (2002); also, see detector section in J. Brodzicka *et al.*, Prog. Theor. Exp. Phys. (2012) 04D001.

[40] S. Kurokawa and E. Kikutani, Nucl. Instrum. Methods Phys. Res., Sect. A **499**, 1 (2003), and other papers included in this volume; T. Abe *et al.*, Prog. Theor. Exp. Phys. (2013) 03A001 and following articles up to 03A011.

[41] D. J. Lange, Nucl. Instrum. Methods Phys. Res., Sect. A **462**, 152 (2001).

[42] T. Sjöstrand *et al.*, Comput. Phys. Commun. **135**, 238 (2001).

[43] R. Brun *et al.*, GEANT, CERN Report No. DD/EE/84-1 (1984).

[44] E. Nakano, Nucl. Instrum. Methods Phys. Res., Sect. A **494**, 402 (2002).

[45] M. Feindt and U. Kerzel, Nucl. Instrum. Methods Phys. Res., Sect. A **559**, 190 (2006).

[46] H. Nakano, Ph.D Thesis, Tohoku University (2014) Chapter 4, unpublished, https://tohoku.repo.nii.ac.jp/?action=pages_view_main&active_action=repository_view_main_item_detail&item_id=70563&item_no=1&page_id=33&block_id=38.

[47] H. Albrecht *et al.* (ARGUS Collaboration), Phys. Lett. B **229**, 304 (1989).

[48] S. S. Wilks, Ann. Math. Stat. **9**, 60 (1938).

[49] Considering the possible change of $\mathcal{B}(\Lambda_c^+ \to pK^-\pi^+)$ in the future, we provide $\mathcal{B}(B^0 \to K^0\Lambda_c^+\bar{\Lambda}_c^-)\mathcal{B}(\Lambda_c^+ \to pK^-\pi^+)^2 = (1.55 \pm 0.29 \pm 0.11) \times 10^{-6}$ and $\mathcal{B}(B^0 \to \Xi_c(2930)^+\bar{\Lambda}_c^-)\mathcal{B}(\Xi_c(2930)^+ \to K^0\Lambda_c^+)\mathcal{B}(\Lambda_c^+ \to pK^-\pi^+)^2 = (9.18 \pm 2.0 \pm 0.72) \times 10^{-7}$, where the first errors are statistical and the second systematic with the uncertainty on $\mathcal{B}(\Lambda_c^+ \to pK^-\pi^+)$ omitted. The 90% C.L. upper limits on $\mathcal{B}(B^0 \to K^0Y(4660))\mathcal{B}(Y(4660) \to \Lambda_c^+\bar{\Lambda}_c^-)\mathcal{B}(\Lambda_c^+ \to pK^-\pi^+)^2$ and $\mathcal{B}(B^0 \to K^0Y_\eta)\mathcal{B}(Y_\eta \to \Lambda_c^+\bar{\Lambda}_c^-)\mathcal{B}(\Lambda_c^+ \to pK^-\pi^+)^2$ are 2.0×10^{-6} and 1.3×10^{-6}, respectively.